Article:
Jovaní, M., Beltrán-Mir, H., Cordoncillo, E. et al. (2017) Atmosphere- and Voltage-Dependent Electronic Conductivity of Oxide-Ion-Conducting Zr1-xYxO2-x/2 Ceramics. Inorganic Chemistry, 56 (12). pp. 7081-7088. ISSN: 0020-1669

https://doi.org/10.1021/acs.inorgchem.7b00673

ATMOSPHERE- AND VOLTAGE- DEPENDENT ELECTRONIC CONDUCTIVITY OF OXIDE ION CONDUCTING $Zr_{1-x}Y_xO_{2-x/2}$ CERAMICS

Marc Jovaní,[a] Héctor Beltrán-Mir,[a] Eloisa Cordoncillo[a] and Anthony R. West[b]

[a]Departamento de Química Inorgánica y Orgánica, Universidad Jaume I, Avda. Sos Baynat s/n, 12071 Castellón, Spain.

[b]Department of Materials Science & Engineering, University of Sheffield, Mappin Street, Sheffield, S1 3JD, UK.

Abstract

Cubic, fluorite-structured solid solutions $Zr_{1-x}Y_xO_{2-x/2}$, YSZ, x=0.4-0.7, were prepared by sol-gel synthesis. Impedance measurements on pellets of approximate density 85% sintered at 1300 ºC for 24 h, showed strong evidence of oxide ion conduction with an inclined Warburg spike at low frequencies and capacitance values ~10^{-6} Fcm^{-1} at 40 Hz. Arrhenius plots of total pellet conductivities were linear with activation energies 1.4 to 1.56 eV. Conductivity decreased with x and was 2 to 4 orders of magnitude lower than with optimised YSZ, x=0.08. On changing the atmosphere from N_2 to O_2 during impedance measurements, two reversible effects were seen: the Warburg spike contracted greatly and the sample resistance decreased. These effects were more noticeable at higher x and are attributed to the introduction of *p*-type electronic conduction, in parallel with pre-existing oxide ion conduction. A similar reversible result was observed on application of a *dc* bias during impedance measurements. On either increasing pO_2 or application of a *dc* bias, hole creation is believed to arise by ionisation of underbonded oxide ions situated near the Y^{3+} dopant ions. The ionised electrons are trapped at surface oxygen species and the holes that are left on oxygen are responsible for *p*-type conduction. The electrolytic domain of x=0.4-0.7 extends up to approximately 10^{-2} atm O_2 before *p*-type conduction is observed. The upper pO_2 limit of the electrolytic domain of x=0.08 is not known but is likely to be close to or slightly above 1 atm O_2.

Keywords: $Y_2Zr_2O_7$; YSZ; electronic conduction; atmosphere/voltage dependence

Introduction

Yttria-stabilised zirconia is the most widely-used oxide ion conductor in solid oxide fuel cells, SOFCs, because of its high conductivity, resistance to reduction, good mechanical strength and stability at high temperatures [1]. The key to this application is the high concentration of mobile anion vacancies created to charge-compensate for introduction of Y^{3+} dopant onto the Zr^{4+} sites. YSZ is a solid solution series of general formula $Zr_{1-x}Y_xO_{2-x/2}$ which has the fluorite structure in which the concentration of oxygen vacancies depends on the value of x. According to the ZrO_2-Y_2O_3 phase diagram [2], Fig. 1(a), the cubic YSZ solid solution extends over the composition range $0<x<0.7$ at high temperatures. At lower x values the solid solutions transform rapidly to tetragonal and/or monoclinic structures on cooling. At higher x values the cubic solid solutions should transform or precipitate secondary phases on cooling but transformation rates may be very slow. The coordination numbers of Zr and Y, which are disordered, depend on x and are less than the ideal value of 8 in the fluorite structure [3]. The cation distribution may not be completely random, however; in composition x = 0.5, corresponding to formula $Y_{0.5}Zr_{0.5}O_{1.75}$, there is a preference for a higher coordination number for Y of 7.2 compared to 6.8 for Zr [3]. Composition x = 0.5 is sometimes referred to as a pyrochlore [4], but diffraction data and crystal structure modelling [5] show little evidence of a pyrochlore structure apart from this indication of a non-random cation distribution.

The composition most widely used in SOFC applications with highest oxide ion conductivity is x=0.08, and is labelled as YSZ08 in this work [1]. At higher x, oxygen vacancy

concentration increases, but defect interactions are held responsible for mobile ion trapping leading to reduction in conductivity and increase in activation energy [6]. For instance, x=0.5 has oxide ion conductivity, 3.75 x 10^{-3} Scm^{-1} at 800 ºC [7] compared to 2.50 x 10^{-2} Scm^{-1} [1], for YSZ08 used in SOFCs.

For all oxide ion conducting solid electrolytes, the electrolytic domain is limited at low oxygen partial pressures, pO_2, by the onset of *n*-type electronic conduction and at high pO_2 by the onset of *p*-type conduction, as shown schematically in Fig 1(b) [8]. YSZ08 is generally regarded as stable down to a pO_2 of 10^{-20} atm which leads to its use as electrolyte in contact with the anode and reducing atmospheres. Little information is available on the upper pO_2 limit of the electrolytic domain for YSZ08, probably because of the difficulty in achieving a wide range of pO_2 values greater than atmospheric pressure. Nevertheless, in the *p*-type region, and using Kroger-Vink notation, it is assumed that uptake of oxygen may occur by a mechanism summarised as:

$$V_o^{\cdot\cdot} + 1/2O_2 \rightarrow O_o^x + 2h^{\cdot} \qquad (1)$$

leading to a gradient of +1/4 in plots of log σ vs log pO_2. Usually, holes are assumed to be located on transition metal ions, present either as controlled dopants or unavoidable impurities, but direct evidence for the site of hole location seems not to be available.

Recently, Masó and West [9] demonstrated that electronic conduction is introduced into YSZ08 under the action of a small *dc* bias at high temperature in air. Similar conductivity changes were seen with acceptor-doped titanate perovskites including Ca-, Zn- and Mg-doped $BaTiO_3$ [10-12] and Ca-doped $BiFeO_3$ [13], which all show enhanced conductivity on either increasing pO_2 in the measuring atmosphere or application of a small *dc* bias. The enhanced conductivity was attributed to ionization of underbonded O^{2-} ions in the vicinity of

acceptor dopants leading to hole creation on oxygen which conceptually, is the same as the creation of O^- ions:

$$O_o^x \rightarrow O_o^{\cdot} + e' \quad (2)$$

The O^- ions are responsible for the enhanced electronic conductivity, which is *p*-type, since the ionized electrons have been immobilized at sample surfaces by participating in one, or more, of the equilibria shown in:

$$O_2(g) \leftrightarrow O_2(ads) \overset{e^-}{\leftrightarrow} O_2^- \overset{e^-}{\leftrightarrow} O_2^{2-} / 2O^- \overset{e^-}{\leftrightarrow} 2O^{2-} \text{ (surface)} \leftrightarrow 2O^{2-} \text{ (bulk)} \quad (3)$$

The *p*-type conduction in the acceptor-doped titanate perovskites is thermally activated which means that the holes are localised rather than delocalised in the valence band. It is a logical step to refer to the holes localized on oxygen as O^- ions, therefore.

Although the conductivity of YSZ with x = 0.08 is not sensitive to pO_2 in atmospheres such as O_2, N_2 or air at atmospheric pressure, preliminary tests on compositions with higher x showed that their conductivity is indeed, sensitive to pO_2. The present work reports a systematic study of the conductivity of YSZ with $0.4<x<0.7$, to determine the effects of pO_2 and *dc* bias on the electrical properties.

Experimental

Four compositions based on the general formula $Zr_{1-x}Y_xO_{2-x/2}$, with x = 0.4, 0.5, 0.6 and 0.7 and labelled YSZ4, YSZ5, YSZ6 and YSZ7 respectively, were prepared by a polymeric sol-gel procedure using $Y(OOCCH_3)_3 \cdot H_2O$ (99.9%, Strem Chemicals) and $Zr(OCH_2CH_2CH_3)_4$ (70% Sigma-Aldrich*)* as precursors. All reagents were of analytical grade and used without further purification. Absolute ethanol (Scharlab, 99.9%) was used as solvent with the necessary amount of acetylacetone, acacH (99% Alfa Aesar) as a stabilizing agent for the Zr

alkoxide precursor. The Zr alkoxide was dissolved in an ethanol-acetylacetone mixture (acacH:Zr molar ratio 4:1), the $Y(OOCCH_3)_3 \cdot H_2O$ added, the mixture stirred for 10 min and then transferred to a balloon flask and heated at 70 ºC for 72 h. A transparent gel formed and was dried in air under an IR lamp at room temperature for approximately 1 day. Finally, the dry gel was ground with an agate mortar and pestle, decomposed by heating at 5 ºC min^{-1} to 500 ºC, left at 500 ºC for 1 h and then heated to 1300 ºC at the rate of 5 ºC min^{-1} with a final hold at 1300 ºC for 12 h. Powder samples were cooled, crushed and pressed into pellets of 5 mm diameter at 1 ton by uniaxial pressing, reheated at 1300 ºC for 24 h and cooled slowly inside the furnace. The four compositions chosen lie in the fluorite-structure phase field at high temperatures, as shown in Fig. 1(a). Pellet densities for all compositions were ~85%.

The phase(s) present were analyzed by X-ray powder diffraction, XRD, using a Bruker D4 Endeavor diffractometer, Karlsruhe, Germany CuKα radiation. Data were collected by step-scanning from $2\theta = 20$ to 70^{o} with a step size of 0.03^{o} and 6 s counting time at each step. The cubic lattice parameter was determined by least-squares refinement for reflections in the range $15 < 2\theta < 70$, using WinXPow version 1.06 (Darmstadt, Germany). Scanning electron micrographs of the pellets were taken on a field emission scanning electron microscope (FE-SEM) JEOL 7001F, equipped with a spectrometer for energy dispersion analysis of X-rays (EDX) from Oxford instruments, using acceleration voltage 15 kV. The samples were deposited on an Al holder and coated with Pt.

For electrical property measurements, electrodes were fabricated on opposite pellet faces from Pt paste (Pt Ink 6082, Metalor, Barcelona, Spain), which was dried and decomposed by gradually heating to 900 ºC. Samples with electrodes attached were placed in a conductivity jig and measured using an Agilent 4294A (Agilent, Madrid, Spain) analyzer over the

frequency range 40 Hz to 13 MHz and temperature range, room temperature to 900 ºC. Impedance data were corrected for overall pellet geometry and are reported in units of specific resistance: ohm cm and capacitance: Fcm^{-1}; data were not corrected for the geometry of regions such as grain boundaries since this was not known accurately. Data were not corrected for sample porosity. In order to avoid any effect of water and therefore, any possible proton conduction, impedance data were recorded in dry atmospheres. Measurements in atmospheres of different pO_2 were carried out in a specially-designed cell fitted with a built-in zirconia probe (MicroPoas by SETNAG) next to the sample, to measure the pO_2 value.

Results

Pellets fired at 1300 $^{\circ}$C for 24 h were ground and analysed by XRD. All samples were single phase and were indexed on a cubic unit cell, space group Fm-3m, fully consistent with literature data. XRD data for x = 0.5 are shown in Fig. 2(a). There was no evidence of a possible pyrochlore structure, whose XRD pattern is expected to contain extra peaks, arrowed, at 2θ = 36.3 and 43.6 compared to the defect fluorite pattern [14]. Lattice parameters as a function of x, inset of Fig 2(a), showed linear increase with x.

The structure of the YSZ solid solutions therefore contains a disordered mixture of Y^{3+} and Zr^{4+} distributed over the 8-coordinate sites of the fluorite structure, with some oxide ion sites vacant, depending on composition x. From Fig 1(a), cubic solid solutions at 1300 ^{o}C are expected to form over the range $0.15 \leq x \leq 0.52$ [2,15,16]. Our results showed single phase cubic solid solutions over a more extensive range of compositions including x = 0.6 and 0.7. We do not know at present whether single phase cubic solid solutions at these compositions

are thermodynamically metastable although clearly, they are kinetically stable under the conditions of synthesis used here. These results may be consistent with the possibility to form metastable phases by sol-gel synthesis [17-20]. A typical microstructure of the pellet surface for YSZ5 is shown in Fig 2(b). Similar microstructures and grain sizes in the range 0.2 – 0.8 μm were observed for all compositions. An SEM of a fracture surface through a pellet with the Pt electrode attached is shown in Fig 2(c) for sample YSZ7; the inset of this figure corresponds to a magnification of the YSZ7 microstructure and confirms the expected porosity. A homogenous layer of the Pt electrode, in contact with the sample surface, is observed in this figure, showing that there is no penetration of the electrode into the interior of the sample. EDX mapping showed a homogeneous distribution of Y and Zr with no evidence of impurities for any of the compositions.

A typical set of impedance data, recorded in dry N_2 at 650 ºC and presented in different formats is shown in Fig. 3 for a pellet of YSZ5 sintered at 1300 ºC for 24 h with density 85%. Similar response was observed for all compositions. The impedance complex plane plots (a) show a broad, depressed arc at high frequencies and an inclined spike with some curvature at low frequencies. The total resistance obtained from the intercept of either the arc or the spike on the Z' axis had a value of ~20 kΩcm. The Z''/M'' spectroscopic plots (b) show peaks at high frequencies which are much broader than expected for an ideal Debye peak, indicating some degree of probable electrical inhomogeneity in the sample but without clear separation of bulk and grain boundary impedances.

The plot of log C'/log f (c, d) for the same data at two temperatures, 650 and 823 ºC, shows evidence for a high frequency plateau of value ~10 pF which corresponds to the limiting high frequency permittivity of ~ 112. The C' values increase with decreasing frequency, with some

evidence for a poorly-resolved intermediate plateau at ~ 30 pF. This value is too small for it to represent a conventional grain boundary since it corresponds to a significant volume fraction of the sample. Instead, we attribute it to either a combination of a constriction grain boundary associated with sample porosity and possible inhomogeneity in distribution of the Y^{3+} dopant or to a dipole orientation-related impedance such as was reported for YSZ08 [21]. Further studies are in progress to understand the nature of this impedance.

With decreasing frequency, C' increases rapidly to reach a value of approximately 1μF at 40 Hz and 823ºC (d); this value is typical of ion blocking at a sample-electrode interface and formation of a double layer capacitance. The inclined spike shown in (a) at low frequencies is attributed to diffusion of oxygen molecules towards and away from sample-electrode interfaces, which therefore places a limit on the rate of oxygen exchange reactions that occur during low frequency measurements. Although this spike, attributed to a Warburg impedance, is not directly associated with oxide ion conduction, it is nevertheless an intrinsic component of redox reactions involving oxygen and is an indirect indication of oxide ion conduction. We therefore interpret the low frequency impedance data to indicate that conduction is primarily by oxide ions but with the possibility of a small amount of electronic conduction (see later).

From data such as these, total sample resistances were obtained from intercepts of either the arc or the Warburg spike on the Z' axis and are shown as conductivity Arrhenius plots as a function of reciprocal temperature in Fig. 4; literature data for YSZ, x=0.08 [22], are shown for comparison. The total conductivity of YSZ solid solutions decreases with x and is 2 to 4 orders of magnitude lower than that of YSZ with x=0.08. In addition, the activation energy increases with x. It is possible that the bulk conductivities are somewhat higher than the total conductivities shown in Fig 4 since either grain boundary constriction impedances or dipole

reorientation impedances are included in the total resistance values; also, conductivities were not corrected for sample porosity. The impedance measurements were obtained on both cooling and heating and the data were reproducible, showing linear behaviour.

The data shown in Figs. 3 and 4 were recorded in an atmosphere of dry N_2 with a pO_2 value of approximately 10^{-4} atm. Data are shown in Fig. 5 for pellets of each composition measured in different atmospheres. Data were measured first in dry N_2 ($pO_2 \sim 10^{-4}$ atm: Hector check); the atmosphere was then changed to dry O_2 (pO_2 ~1 atm) and the system allowed to stabilise for a few minutes before impedance data were collected in O_2. Two effects are seen in the impedance complex plane plots, (a-d), which were reversible on switching between O_2 and N_2. First, the Warburg spike contracts greatly and becomes a small arc in O_2; second, the total sample resistance decreases. The effects were more noticeable with higher x compositions. It is most unlikely that these two phenomena could be attributed to changes in oxide ion conductivity in the samples simply as a consequence of changing pO_2 in the measuring atmosphere.

Changes in conductivity with pO_2 are widely used as an indication of extrinsic electronic conduction in materials since reactions such as eq'n 1 lead to changes in electronic carrier concentration, of either electrons or holes. We therefore interpret the data shown in Fig 5 to indicate the presence of *p*-type conduction when samples are measured in O_2 since chemisorption of oxygen with increasing pO_2 leads to hole creation, eq'n 1. This means that a certain amount of *p*-type electronic conduction [23, 24] occurs in parallel with the pre-existing oxide ion conduction. The electronic conduction must arise from reactions involving O_2 in the atmosphere. Eq'n 1 shows the creation of holes but gives no indication as to their

location. Traditionally, holes are associated with transition metal impurities but we believe that a more likely location, at least in our materials, is underbonded oxide ions.

The loss of the Warburg spike is also attributed to creation of a parallel electronic conduction pathway [9]. It is further emphasised in the capacitance data, insets Fig 5(a-d), in which the large, high-valued low frequency capacitance decreases because it is no longer associated specifically with charge transfer at the thin, double layer interface.

Impedance data were sensitive to pO_2 over the complete temperature range studied, 500-850 ºC and are summarized in Arrhenius plots of total conductivity for one composition, YSZ7 in Fig 6. The data recorded in O_2 are higher by a factor of 2 to 3 with a smaller activation energy and clearly must contain a contribution of both electronic and ionic conductivity. We do not know if the data in N_2 also contain a small electronic component or whether they represent exclusively ionic conduction. These results show that, with reference to Fig 1(b), samples YSZ4 - YSZ7 in air at atmospheric pressure are in the crossover region between the electrolytic domain and *p*-type conduction. At present, we have not performed a detailed determination of the electronic transport number in our compositions, which would allow the contribution of each conduction mechanism to the electrical response to be determined as a function of temperature, pO_2 and x. Different methods are reported in the literature to determine the electronic and ionic components of the conductivity [9, 25].

The effect on impedance data of application of a small *dc* bias, in the range 0.5-2V, was found to be very similar to that of increasing pO_2. A selection of results is shown in Fig 7 for YSZ7 and YSZ4. In (a), data are shown in N_2 and O_2 without an applied bias and in N_2 with 2V bias. The data in O_2 and in N_2 with 2V bias are similar and both show reduced total

resistance and a much reduced Warburg spike. In (b), data are shown for *dc* bias in the range 1–10V; a systematic decrease in both sample resistance and Warburg impedance is observed.

The changes in conductivity with changing pO_2 are not instantaneous but take a few minutes to reach the steady state, as shown in Fig 8 for YSZ5 at 750 ºC. The sample was first equilibrated in N_2 for 24 h and the resistance measured as a function of time on switching to O_2. Once a steady state had been reached, the atmosphere was switched back to N_2; several minutes were needed to reach a steady-state in both directions. Fig 8 therefore corresponds to a continuous time plot with a switch in atmosphere at intermediate time.

Discussion

The electrical properties of YSZ, x=0.4-0.7, without application of a *dc* bias, are consistent with oxide ion conduction, as is, of course, widely-recognised for YSZ08 [26]. The conductivity is lower than that of YSZ08, which is usually used as a ceramic electrolyte in SOFC systems. Although the compositions prepared with higher x have a higher concentration of oxygen vacancies, the reduction in ionic conductivity with increasing x is attributed to trapping of oxygen vacancies in defect complexes associated with the Y^{3+} dopant; this is also consistent with the observed increase in activation energy for ionic conduction in higher x compositions [6].

YSZ08 is used as the ceramic electrolyte in SOFCs in part because it is very stable to reduction. However, it has recently been shown that electronic conduction can be induced in YSZ08 by application of a small bias voltage [9]. This causes YSZ08 to become a mixed

conductor with, for instance, an electronic transport number, t_e, of 0.5 with 10 V bias at ~ 550 ºC. The electronic conductivity is lost on removal of the *dc* bias.

In the present study, we report a similar dependence of conductivity on *dc* bias, but also show that the conductivity is sensitive to pO_2. The onset of electronic conductivity is shown by two changes to the impedance data: first, the Warburg spike is greatly reduced and second, the total sample resistance is reduced. Reversible changes of a similar nature are seen with both an increase in pO_2 and a *dc* bias. There is no evidence from the literature that YSZ08 is sensitive to an increase in pO_2, although it is sensitive to *dc* bias [9]. From the results presented here, the introduction of electronic conductivity becomes easier with increasing x and it seems highly probable, therefore, that YSZ08 itself will be sensitive to pO_2 at pressures just above 1 atm O_2. This result has clear significance for the use of YSZ-based materials either in an oxygen-rich atmosphere or in the presence of a bias voltage.

The sensitivity of the total sample conductivity to changes in pO_2, Fig 5, is evidence that the electronic conduction mechanism is *p*-type. This was presumed, but not established, in the earlier YSZ results [9] and follows previous studies of acceptor-doped titanate perovskites which showed enhanced *p*-type conductivity with a *dc* bias. In those studies [9-12], the mechanism of hole creation was attributed to ionisation of underbonded oxide ions associated with lower-valence acceptor dopants. The holes that are created are localised on oxygen, as O^- ions, and are responsible for the thermally-activated *p*-type conduction. The Y^{3+} component of the YSZ solid solutions may be regarded also as an acceptor dopant in which Y^{3+} substitutes for Zr^{4+}; oxide ions in the immediate vicinity of Y^{3+} are effectively underbonded and can be readily ionised. The effect of increasing x is to increase the Y^{3+}

concentration and therefore, the concentration of underbonded oxide ions; this may account for the increased sensitivity to pO_2 that is seen with increasing x.

The chemisorption on sample surfaces that takes place with increasing pO_2 is a commonly-used diagnostic for extrinsic conductivity and to distinguish *p*-type from *n*-type conduction. Using eq'n 1 to represent the chemisorption, electrons are removed from the sample, presumably close to the absorption sites, to form reduced oxygen species. In reality, several equilibria at sample surfaces may be involved, as indicated schematically in eq'n 3, giving rise to species such as superoxide O_2^-, peroxide, O_2^{2-}, O^- and finally O^{2-} ions, whose net negative charges are balanced by the holes that are created as lattice O^- ions. Several of these equilibria require electrons and hence, with increasing pO_2, lead an overall increase in *p*-type conductivity, as shown in Fig. 8. These processes commence at any part of sample surface exposed to the atmosphere.

Similar behaviour to that seen with increasing pO_2 is observed on application of a small *dc* bias which, for voltages of 1-2 V, is below the probable decomposition voltage of the samples. This behaviour may also be interpreted in terms of the equilibria shown in eq'n 3 as these equilibria are driven to the right hand side by a positive bias, leading to removal of electrons from the sample and an increase in *p*-type conduction. The positive electrode is therefore responsible for the observed conductivity changes and there is no evidence of any opposite effect occurring at the negative electrode, which would lead to negative charge injection. Thus, if charge injection were to occur, this would lead to the onset of *n*-type conduction, as represented by the cross-over region at low pO_2 shown in Fig 1(b), in contrast to the observed *p*-type behaviour. There are reported instances of blackening and electronic conduction in YSZ ceramics which can be attributed to charge injection from the negative

electrode under highly reducing conditions. If changes to the sample do occur at the negative electrode under *dc* bias, they are not directly responsible for the effects reported here. Thus, we also exclude the possibility of Schottky barrier formation and charge injection resulting from a reduction in barrier height on application of the *dc* bias.

Conclusions

There is huge interest in yttria-stabilised zirconia, YSZ as the ceramic electrolyte for solid oxide fuel cell applications because, as well as its high oxide ion conductivity, it is very resistant to reduction; consequently, its 'electrolytic window' extends down to very low partial pressures of oxygen before it shows the onset of *n*-type conduction. This work concerns the upper limit of the electrolytic window before the onset of *p*-type conduction.

Conductivity measurements in different atmospheres show that with increasing Y content, YSZ compositions x=0.4-0.7 are already at the cross-over between electrolytic and *p*-type conduction on switching between N_2 and O_2 atmospheres; a similar conclusion is reached on conducting impedance measurements in the presence of a small dc bias, and is attributed to the creation of holes on underbonded O^{2-} ions associated with the Y^{3+} acceptor dopant. We do not know the value of the activation energy for the electronic component in the *p*-type region, but it is probably non-zero which means that the holes are localised on oxygen and not delocalised in the valence band structure. The activation energy of YSZ7 in O_2, 1.48 eV, is somewhat less than that in N_2, 1.56 eV, Fig. 6 and therefore, the activation energy for *p*-type conduction is presumed to be less than that for oxide ion conduction.

These results are significant for several reasons:

First, they demonstrate that, depending on Y content, YSZ samples may lose their exclusive oxide ion conductivity either in the presence of a small applied voltage or with increasing oxygen partial pressure. For samples of YSZ08 used in SOFC applications, the onset of the *p*-type conduction is likely to occur at oxygen partial pressures close to, or slightly above 1 atm.

Second, they demonstrate an alternative method by which electronic conductivity can be introduced into YSZ. Most focus in the literature is on the onset of possible *n*-type conductivity with either reducing atmospheres or decreasing pO_2, whereas we demonstrate the very easy introduction of *p*-type conductivity under near-ambient conditions and in the presence of small *dc* voltages.

Third, they highlight that the mechanism of hole creation must involve redox activity of underbonded oxide ions, which challenges the widely-held belief that oxygen in oxides is present solely as the double negative oxidation state. In high purity chemicals such as used here, there seems to be no other possibility for location of the holes.

Fourth, the ready introduction of *p*-type conductivity into YSZ-based materials may have significant consequences for their application as electronically-insulating ceramics in either a high pO_2 environment or in the presence of extraneous voltages.

Acknowledgements

MJ, HB, EC thank the "Universitat Jaume I" project No. P1 1B2013-25 and Ministerio de Economía, Industria y Competitividad, Project No. MAT2016-80410-P for financial support. MJ also thanks the Universitat Jaume I for a fellowship.

References

[1] Stambouli, A.B.; Traversa, E.. Solid oxide fuel cells (SOFCs): a review of an environmentally clean and efficient source of energy. *Renewable and Suitainable Energy Reviews* **2002**, 6, 433–455.

[2] Chen, M.; Hallstedt, B.; Gauckler, L. J. Thermodynamic modeling of the ZrO_2–$YO_{1.5}$ system. *Solid State Ionics* **2004**, 170, 255-274.

[3] Zhang, Z.; Middleburgh, S.C.; De los Reyes, M.; Lumpkin, G.R.; Kennedy, B.J.; Blanchard, P.E.R.; Reynolds, E.; Jang, L.Y. Gradual Structural Evolution from Pyrochlore to Defect-Fluorite in $Y_2Sn_{2-x}Zr_xO_7$: Average vs Local Structure. *J. Phys. Chem. C.* **2013,** 117, 26740–26749.

[4] Panero, W.; Stixrude, L.; Ewing, R. First-principles calculation of defect-formation energies in the $Y_2(Ti,Sn,Zr)_2O_7$ pyrochlore. *Phys. Rev. B.* **2004**, 70, 054110-1-11.

[5] Du, Q.; Zhou, G.; Zhou, J.; Jia, X.; Zhou, H. Enhanced luminescence of novel $Y_2Zr_2O_7:Dy^{3+}$ phosphors by Li^+ co-doping. *J. Alloys Compd.* **2013**, 552, 152–156.

[6] Kilner, J.A.; Steele, B.C.H. Nonstoichiometric Oxides, Academic Press, 1981.

[7] Kumar, M.; Raj, I.A., Pattabiraman, R. $Y_2Zr_2O_7$ (YZ)-pyrochlore based oxide as an electrolyte material for intermediate temperature solid oxide fuel cells (ITSOFCs)-Influence of Mn addition on YZ. *Mater. Chem. Phys.* **2008**, 108, 102–108.

[8] West, A.R. Solid State Chemistry and its Applications, Second Edition, Wiley 2014.

[9] Masó, N.; West, A.R. Electronic Conductivity in Yttria-Stabilized Zirconia under a Small dc Bias. *Chem. Mater.* **2015**, 27, 1552–1558.

[10]. Masó, N.; Prades, M.; Beltrán, H.; Cordoncillo, E.; Sinclair, D.C.; West, A.R. Field enhanced bulk conductivity of acceptor-doped $BaTi_{1-x}Ca_xO_{3-x}$ ceramics. *Appl. Phys. Lett.* **2010**, 97, 062907-1-3.

[11] Beltrán, H.; Prades, M.; Masó, N.; Cordoncillo, E.; West, A.R. Voltage-Dependent Low-Field Bulk Resistivity in $BaTiO_3$:Zn Ceramics. *J. Am. Ceram. Soc.* **2010,** 93, 500–505.

[12] Prades, M.; Masó, N.; Beltrán, H.; Cordoncillo, E.; West, A.R. Field enhanced bulk conductivity of $BaTiO_3$:Mg ceramics. *J. Mater. Chem.* **2010**, 20, 5335–5344.

[13] Masó, N.; Beltrán, H.; Prades, M.; Cordoncillo, E.; West, A.R. Field-enhanced bulk conductivity and resistive-switching in Ca-doped $BiFeO_3$ ceramics. *Phys. Chem. Chem. Phys.* **2014,** 16, 19408-19416.

[14] Zou, X.; Zhou, G.; Yi, H.; Zhang, G.; Wang, S. Fabrication of Transparent $Y_2Zr_2O_7$ Ceramics from Combustion-Synthesized Powders. *J. Am. Ceram. Soc.* **2011**, 94, 1002–1004.

[15] Du, Y.; Jin, Z.; Huang, P. Thermodynamic Assessment of the ZrO_2-$YO_{1.5}$ System. *J. Am. Ceram. Soc.* **1991**, 74, 1569-1577.

[16] Subramanian, M.A.; Aramavidan, G.; Subba Rao, G.V. Oxide pyrochlores - A review. *Prog. Solid State Chem.* **1983**, 16, 55-143.

[17] Brinker, C.J.; Scherer, G.W.; Sol–Gel Science, Academic Press, New York, 1990.

[18] Mackenzie, J.D. Unusual non-crystalline solids from gels in 2004. *J Non-Cryst. Solids* **1985**, 73, 631-637.

[19] Viazzi, C.; Bonino, J.P.; Ansart, F.; Barnabé, A. Structural study of metastable tetragonal YSZ powders produced via a sol–gel route. *J. Alloy Compd.* **2008**, 452, 377-383.

[20] Beltrán, H.; Gómez, B.; Masó, N.; Cordoncillo, E.; West, A.R. Electrical properties of ferroelectric $BaTi_2O_5$ and dielectric $Ba_6Ti_{17}O_{40}$ ceramics. *J. Appl. Phys.* **2005**, 97, 084104-1-6.

[21] Hernandez, M.A.; West, A.R. Dipolar relaxation and impedance of an yttria-stabilised zirconia ceramic electrolyte. *J. Mater. Chem. A* **2016**, 4, 1298-1304.

[22] Ren, P.; Masó, N.; Liu, Y.; Ma, L.; Fan, H.; West, A.R. Mixed oxide ion and proton conduction and p-type semiconduction in $BaTi_{0.98}Ca_{0.02}O_{2.98}$ ceramics. *J. Mater. Chem. C* **2013**, 1, 2426-2432.

[23] Jamnik, J.; Maier, J.J. Treatment of the Impedance of Mixed Conductors Equivalent Circuit Model and Explicit Approximate Solutions. *J. Electrochem. Soc.* **1999**, 146, 4183-4188.

[24] Lai, W.; Haile, S.M. Impedance spectroscopy as a tool for chemical and electrochemical analysis of mixed conductors: a case study of ceria. *J. Am. Ceram. Soc.* **2005**, 88, 2979-2997.

[25] Huggins, R.A., Simple method to determine electronic and ionic components of the conductivity in mixed conductors. *Ionics* **2002**, 8, 300-313.

[26] Brune, A.; Lajavardi, M.; Fisler, D.; Wagner Jr., The electrical conductivity of yttria-stabilized zirconia prepared by precipitation from inorganic aqueous solutions. *Solid State Ionics* **1998**, 106, 89-101.

Figure captions

Fig 1. (a) Phase diagram of the ZrO_2-$YO_{1.5}$ system [2]; the compositions prepared in this work are indicated. (b) Schematic ionic and electronic conductivity domains as a function of oxygen partial pressure, pO_2, adapted from reference [8].

Fig 2. (a) XRD pattern and (b) SEM of the pellet surface of YSZ5 sintered at 1300ºC. (c) SEM of the fracture surface of YSZ7 with the Pt electrode attached. Inset in (a): variation in lattice parameter with x. Inset in (c): magnification of the YSZ7 microstructure of the fracture pellet.

Fig 3. (a) Impedance complex plane plot, Z*, (b) Z''/M'' and (c,d) C' spectroscopic plots at different temperatures for YSZ5. Measurements in dry N_2; $\omega = 2\pi f$.

Fig 4. Arrhenius plots of total conductivities for samples sintered at 1300ºC and measured in dry N_2. Error bars are within the size of data points. Activation energies in eV, with errors in the range 0.02-0.05 eV, are shown beside each data set. YSZ08 ceramic sintered at 1600ºC for 6h is included for comparison [22].

Fig 5. Impedance complex plane plots, Z*, with C' spectroscopic plots as insets for all compositions measured in dry N_2 and O_2 at 750ºC.

Fig 6. Arrhenius plots of total conductivity for YSZ7 measured in dry N_2 and O_2. Activation energies in eV are shown beside each data set.

Fig 7. (a) Impedance complex plane plots for YSZ7 measured in dry N_2 and O_2 at 750ºC and with 2V bias voltage in dry N_2. (b) Impedance complex plane plots for YSZ4 measured in dry N_2 after applying different bias voltages at 800ºC.

Fig. 8. Time-dependent total resistivity for YSZ5 at 750ºC in dry (a) O_2 and (b) N_2.

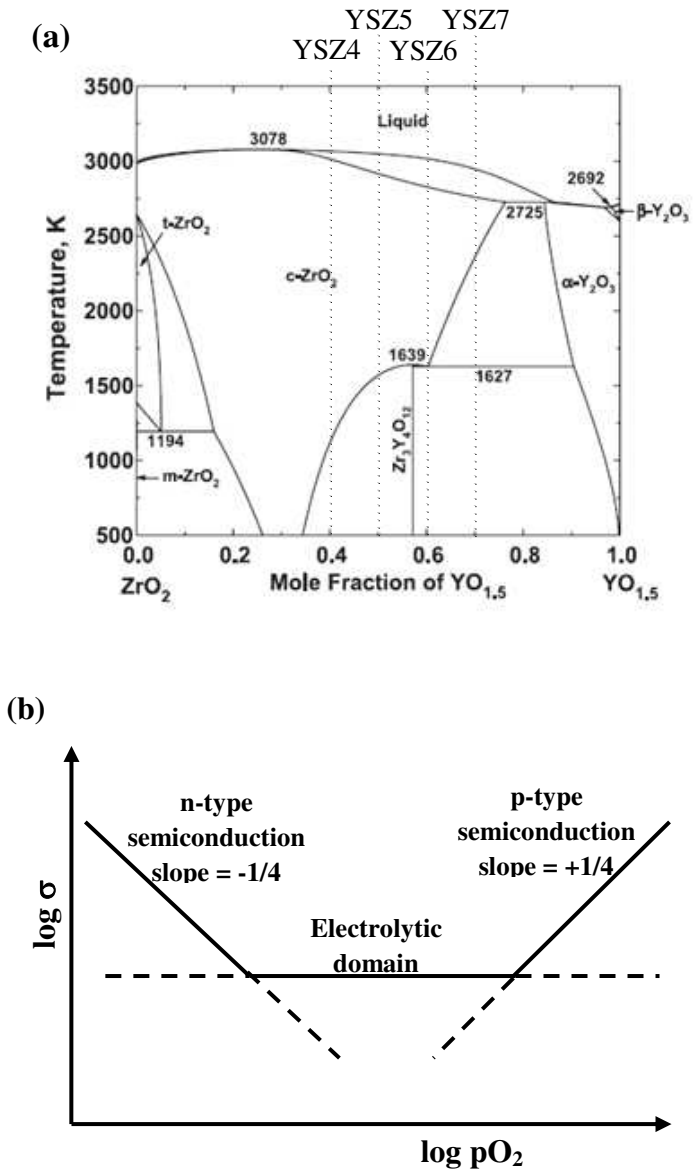
(a)
YSZ5
YSZ7
YSZ4
YSZ6
Liquid
3078
2692
2725
β-Y2O3
t-ZrO2
c-ZrO2
α-Y2O3
1639
1627
1194
m-ZrO2
Zr3Y4O12
Temperature, K
3500
3000
2500
2000
1500
1000
500
0.0
0.2
0.4
0.6
0.8
1.0
ZrO2
Mole Fraction of YO1.5
YO1.5
(b)
n-type
semiconduction
slope = -1/4
p-type
semiconduction
slope = +1/4
Electrolytic
domain
log σ
log pO2

Fig 1.

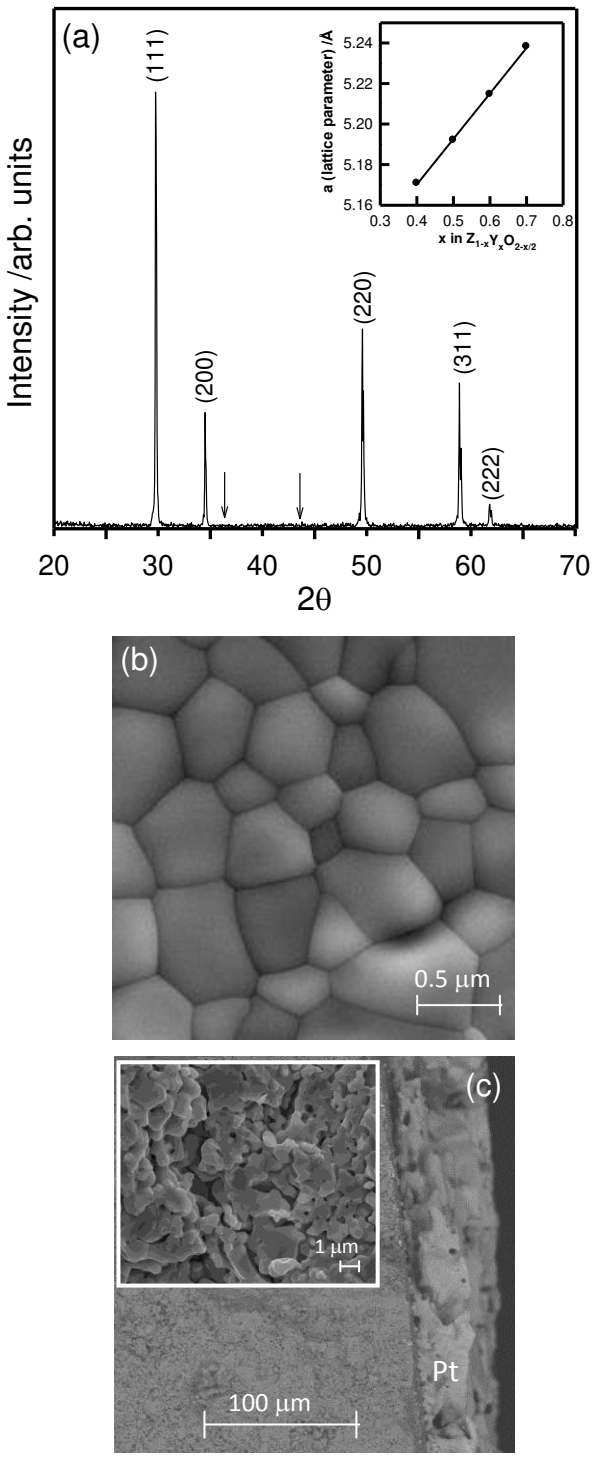
(a)
(111)
(200)
(220)
(311)
(222)
Intensity /arb. units
2θ
20
30
40
50
60
70
a (lattice parameter) /A
5.24
5.22
5.20
5.18
5.16
0.3
0.4
0.5
0.6
0.7
0.8
x in Z1-xYxO2-x/2
(b)
0.5 μm
(c)
1 μm
Pt
100 μm

Fig 2.

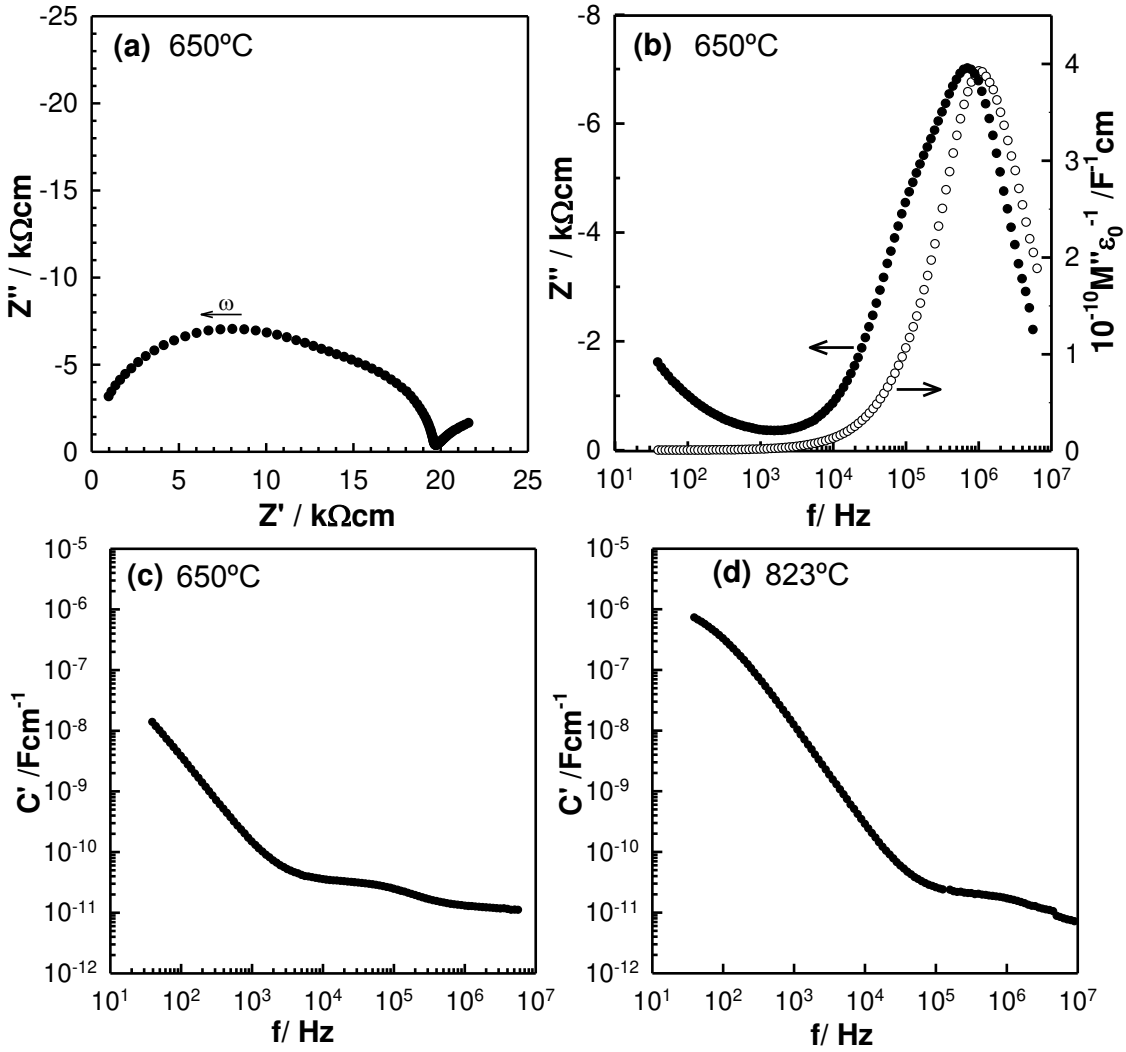
(a) 650ºC
Z'' / kΩcm
Z' / kΩcm
ω
(b) 650ºC
Z'' / kΩcm
10^-10 M'' ε0^-1 /F^-1 cm
f/ Hz
(c) 650ºC
C' /Fcm^-1
f/ Hz
(d) 823ºC
C' /Fcm^-1
f/ Hz

Fig 3.

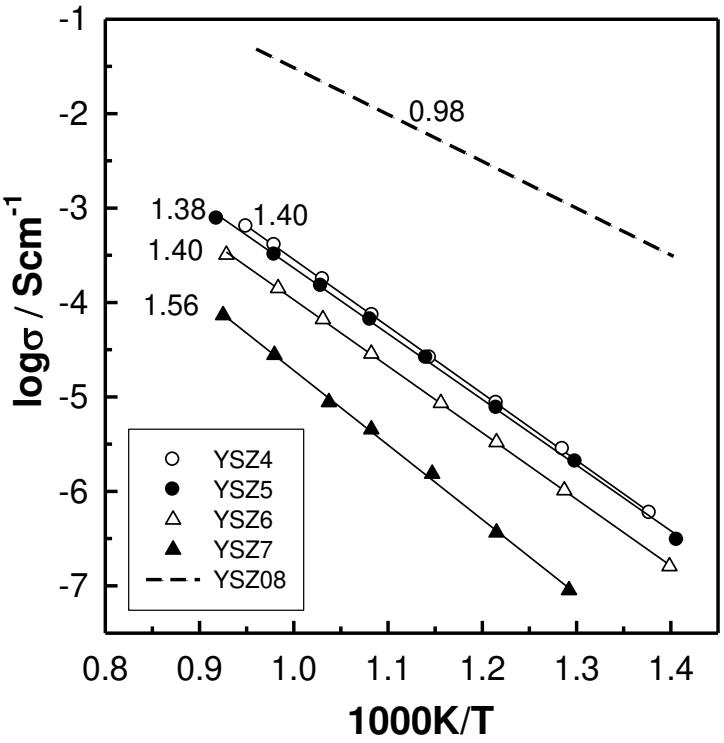
-1
-2
-3
-4
-5
-6
-7
logσ / Scm-1
0.98
1.38
1.40
1.40
1.56
YSZ4
YSZ5
YSZ6
YSZ7
YSZ08
0.8
0.9
1.0
1.1
1.2
1.3
1.4
1000K/T

Fig 4.

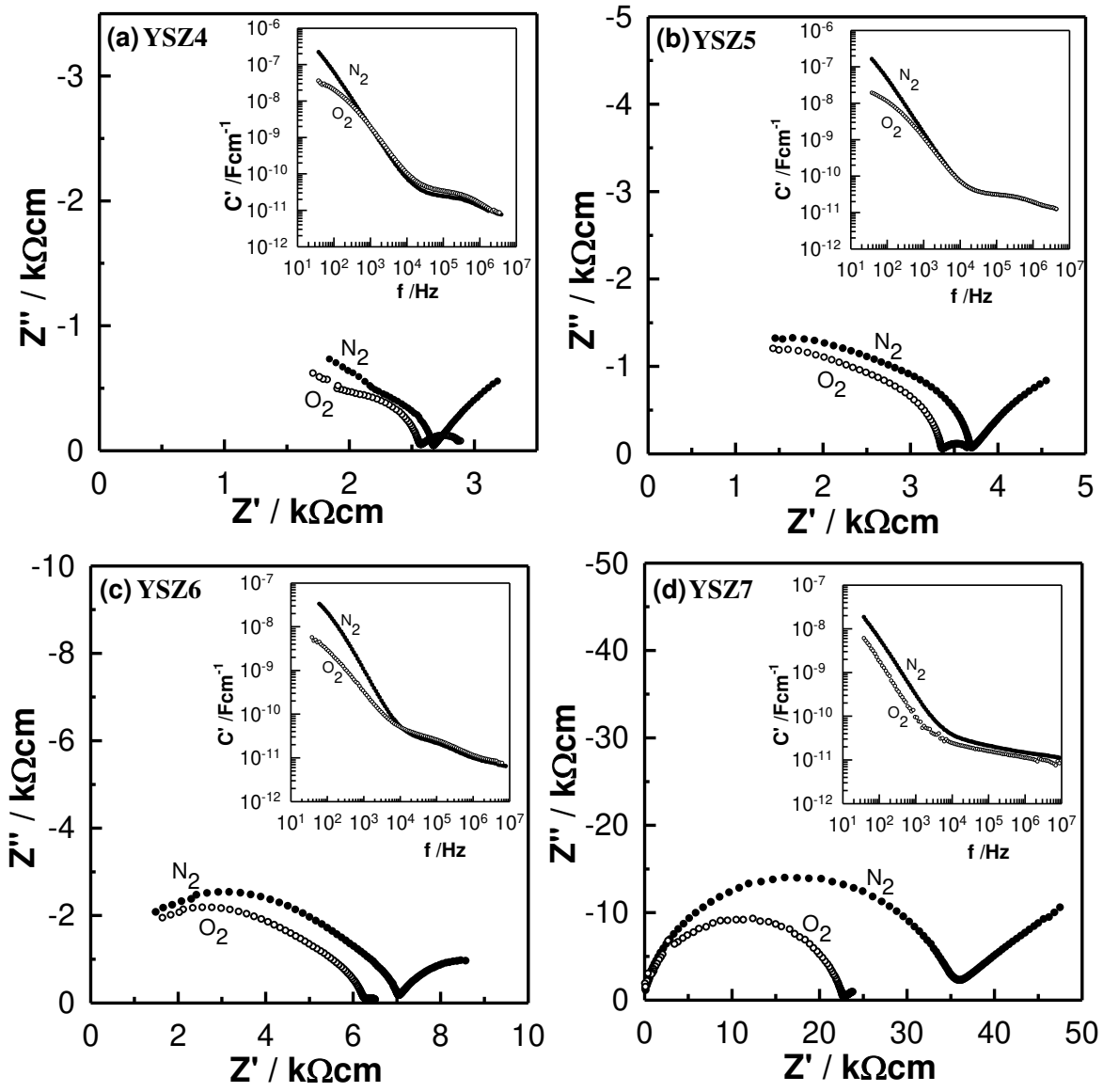

Fig 5.

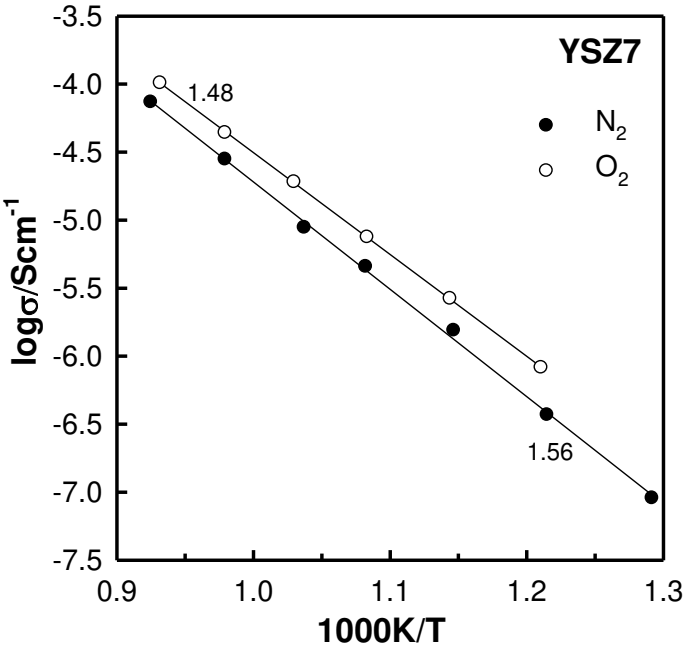
YSZ7
1.48
1.56
N2
O2
logσ/Scm-1
1000K/T
-3.5
-4.0
-4.5
-5.0
-5.5
-6.0
-6.5
-7.0
-7.5
0.9
1.0
1.1
1.2
1.3

Fig 6.

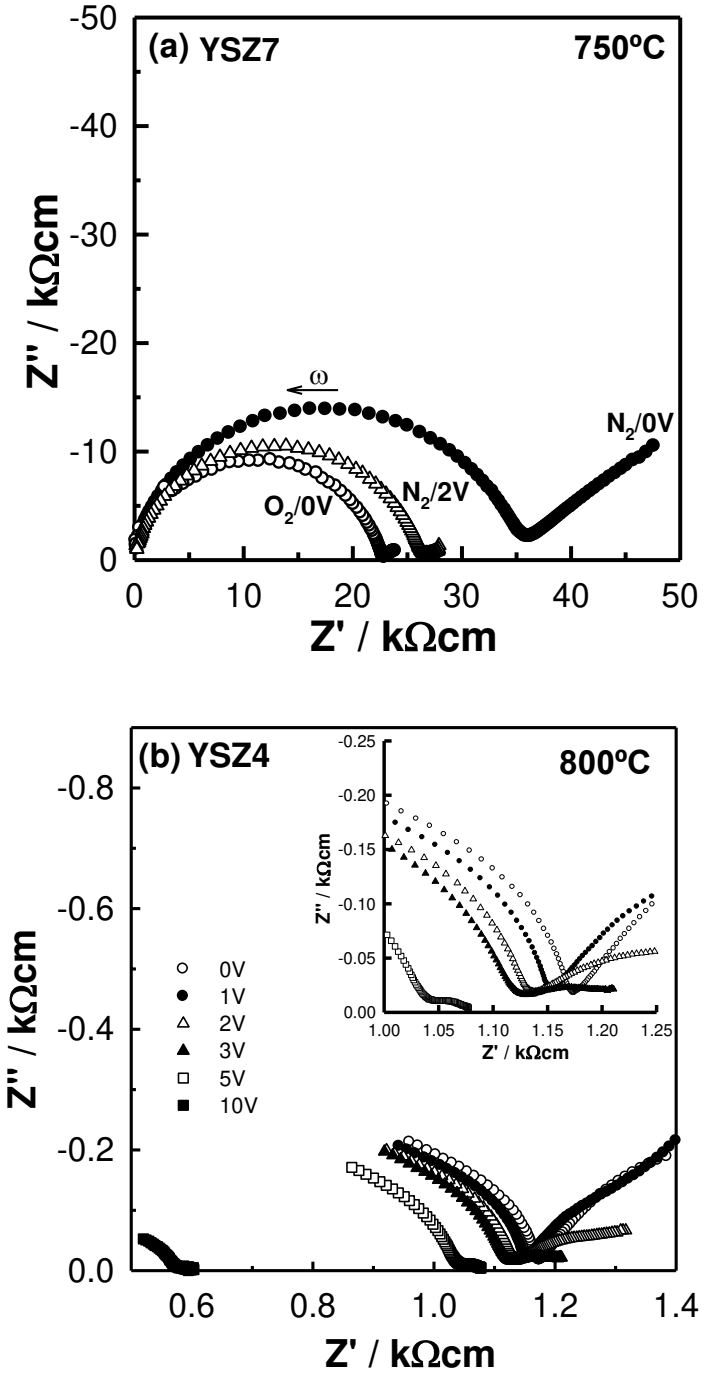
(a) YSZ7
750ºC
ω
N2/0V
N2/2V
O2/0V
Z'' / kΩcm
Z' / kΩcm
(b) YSZ4
800ºC
0V
1V
2V
3V
5V
10V
Z'' / kΩcm
Z' / kΩcm

Fig 7.

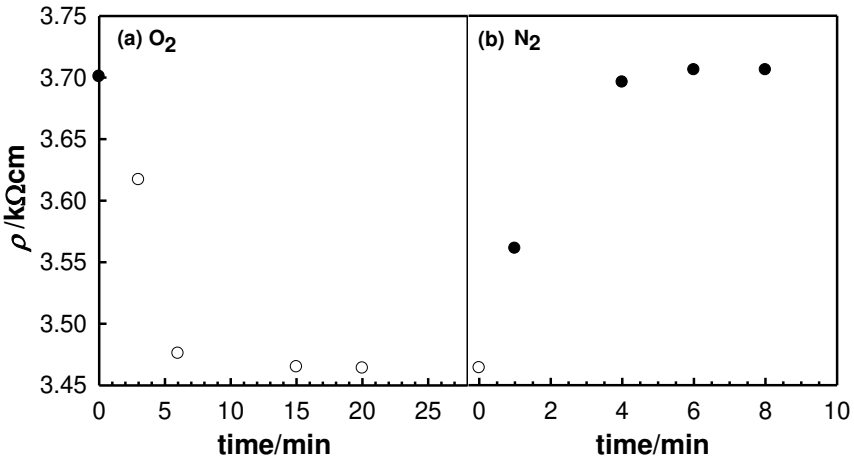
(a) O_2
(b) N_2
ρ /kΩcm
3.75
3.70
3.65
3.60
3.55
3.50
3.45
0
5
10
15
20
25
0
2
4
6
8
10
time/min
time/min

Fig. 8.

TOC graphic and synopsis

Cubic solid solutions based on $Zr_{1-x}Y_xO_{2-x/2}$, x = 0.4-0.7 were prepared by sol-gel synthesis. *p*-type electronic conduction was introduced by increasing pO_2 or *dc* bias voltage. The electrolytic domain extends up to ~10^{-2} atm O_2 before *p*-type conduction is observed, which is different to the known YSZ, x=0.08.

The introduction of *p*-type conductivity into YSZ-based materials may have significant consequences for their application as electronically-insulating ceramics in either a high pO_2 environment or in the presence of extraneous voltages.